Electrical PV Array Reconfiguration Strategy for Energy Extraction Improvement in Grid-Connected PV Systems

Guillermo Velasco-Quesada, *Member, IEEE*, Francisco Guinjoan-Gispert, *Member, IEEE*, Robert Piqué-López, *Member, IEEE*, Manuel Román-Lumbreras, *Member, IEEE*, and Alfonso Conesa-Roca

***Abstract*—This paper applies a dynamical electrical array reconfiguration (EAR) strategy on the photovoltaic (PV) generator of a grid-connected PV system based on a plant-oriented configuration, in order to improve its energy production when the operating conditions of the solar panels are different. The EAR strategy is carried out by inserting a controllable switching matrix between the PV generator and the central inverter, which allows the electrical reconnection of the available PV modules. As a result, the PV system exhibits a self-capacity for real-time adaptation to the PV generator external operating conditions and improves the energy extraction of the system. Experimental results are provided to validate the proposed approach.**

***Index Terms*—Electrical array reconfiguration (EAR), grid-connected photovoltaic (PV) systems, reconfigurable PV systems.**

I. Introduction

PHOTOVOLTAIC (PV) energy generation provides several advantages such as being harmless for the environment and renewable. Furthermore, grid-connected PV energy generation represents a renewable energy-growing alternative that is becoming more competitive due to the new favorable governmental laws and policies recently introduced. For instance, most of the programs supporting PV systems have promoted, among others, the expansion of small residential PV systems up to 5 kWp connected to the single-phase grid primarily installed in roofs [1], [2].

The plant-oriented (PO) configuration is one of the most prevailing PV grid-connected system's architectures due to its simplicity and low cost per peak kilowatt, and assumes a single PV generator (or solar array) formed by a prefixed parallel connection of series-connected modules (also referred to as strings) which is linked to the grid through a single central inverter [1], [2]. The dc power extraction is carried out by the inverter input stage which is generally driven by a maximum power point tracking (MPPT) algorithm in charge to ensure the PV generator operation at its maximum power point whatever the environmental (irradiance and temperature) conditions are.

One of the major sources of power losses in such architecture arises when the PV generator is partially shaded by clouds or by surrounding obstacles such as in the case of urban environments [3]–[6]. These losses are mainly due to the electrical configuration of the PV generator, in particular to the hard-wired series connection of PV modules in each string since a partially shaded module limits the string current where it is connected, thus reducing the maximum available dc power of the PV generator. Furthermore, this power reduction can also occur in case of module failure for the same reasons.

In order to improve the dc power extraction of a partially shaded solar array, several solutions modifying either: 1) the power processing architecture or 2) the PV generator electrical behavior at the solar cells level, have been proposed.

1) The strategy which modifies the power processing architecture is based on a previous association of the available PV modules in several independent PV generators. Each PV generator is formed by the PV modules operating under similar environmental conditions to reduce the current limitation on the strings. Furthermore, the dc power extraction is improved by a modified power processing architecture which shares out the maximum dc power extraction task among as many power processors as independent PV generators are. Depending on the number of PV generators, ac-module inverters [7], [8], string and multistring converters [9], [10], or cascaded full-bridge multilevel [11] topologies are some of the power processing architectures supporting this strategy. It is worth noting that this approach improves the energy efficiency and the reliability of the PV system at expenses of increasing the power stage complexity and cost [12].
2) To avoid these drawbacks, other solutions modify the operation of the PV generator at the solar cells level when partial shades are present, keeping the power processing architecture based on a single power processor (i.e., a single inverter in the case of the PO configuration). The

Manuscript received December 23, 2008; revised May 26, 2009. First published July 24, 2009; current version published October 9, 2009. This work was supported in part by the Spanish Ministry of Science and Technology and in part by the EU (FEDER funds) under Project DPI-2006-15627-C03-01, and was developed at the *URT EdePAE* (Technology Transfer Unit on Power Electronics and Electric Drives) installations of the EUETIB.

G. Velasco-Quesada, R. Piqué-López, and A. Conesa-Roca are with the Departamento de Ingeniería Electrónica, Escuela Universitaria de Ingeniería Técnica Industrial de Barcelona, Universitat Politècnica de Catalunya, 08036 Barcelona, Spain (e-mail: guillermo.velasco@upc.edu).

F. Guinjoan-Gispert is with the Departamento de Ingenieria Electrónica, Escuela Técnica Superior de Ingenieros de Telecomunicación de Barcelona, Universitat Politècnica de Catalunya, 08034 Barcelona, Spain.

M. Román-Lumbreras is with the Departamento de Ingeniería Electrónica, Universitat Politècnica de Catalunya, 08034 Barcelona, Spain.

Color versions of one or more of the figures in this paper are available online at http://ieeexplore.ieee.org.

Digital Object Identifier 10.1109/TIE.2009.2024664

most popular one is well known by the PV modules manufacturers who provide the option to connect bypass diodes in parallel with some subsets of series-connected solar cells assembled in the module. The PV module power improves since these diodes turn-on and release the series-connection current limitation when several of these cells are shaded. However, when bypass diodes are employed the power-to-voltage/current curves of the PV generator exhibit more than one maximum. Consequently, the maximum power extraction requires the use of more sophisticated MPPT algorithms able to disregard local maximums with respect to the absolute one. Unfortunately, commercial inverters rarely include these advanced algorithms [3].

An alternative approach based on an adaptive electrical array reconfiguration (EAR) of solar cells has been recently proposed in [13]. In this paper, the authors introduce a new configuration of the solar cells connections based on a hard-wired fixed part of total-cross-tied array and an adaptive one of independent solar cells, being both parts linked through a controllable matrix of switches. This matrix is controlled in real time to connect the less shaded cells of the adaptive part, in parallel with the more shaded rows of the fixed one. Accordingly, this reconfiguration strategy releases the array current limitation under partial shades and optimizes the output power. The proper operation of this strategy has been experimentally confirmed by the authors in the case of a reconfigurable array directly feeding a resistive load. However, this interesting approach requires the PV module manufacturers commitment to be commercially available in the future.

In contrast, the work here reported proposes a reconfiguration strategy at the PV module level which can be applied to commercial PO grid-connected PV systems available nowadays, i.e., formed by standard PV modules and a single central inverter driven by a conventional MPPT algorithm. The proposed approach is partially inspired in the EAR applied to autonomous PV systems such as cars powered by solar energy [14] and electric engines coupled to water pumps [15]–[17]. As previously reported by the authors of this paper in [18]–[20] and following a similar way as done in [13], the reconfiguration strategy is based on a controllable matrix of switches configuring the PV modules in a single-string of parallel-connected rows connected to the central inverter. Under partial shades or in case of module failure, the matrix control algorithm reconfigures the PV modules to maximize the current of the single string, i.e., the output power of the system.

This paper extends the contents reported in [18]–[20] with a detailed description of the switching matrix design, its implementation, and control in Sections II and III, respectively. Section IV details the experimental setup of a commercial 1.65-kWp grid-connected PV system built following the proposed approach to test the proper operation of the strategy. Subsequently, Section V reports an extended set of experimental results to show the EAR PV system operation. Finally, the last section draws the conclusions of the paper and its contribution to the energy and reliability improvement of PV systems.

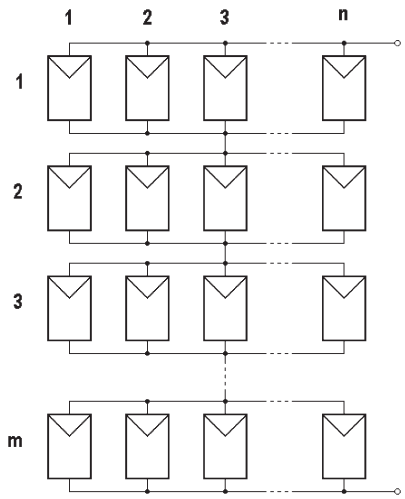

Fig. 1. EAR PV generator topology.

II. Switching Matrix Design

All the available PV modules are assembled in an $m \times n$ matrix structure of a single string of m series-connected rows with n parallel-connected modules per row, as shown in Fig. 1, which will be referred as "EAR PV generator topology."

It is worth noting that the maximum available dc power at the output of the PV generator will depend on the operating conditions of each module (i.e., irradiance, temperature, and electrical characteristics) and on their location in the matrix structure. This property can be used to maximize the dc output power by properly relocating the PV modules within the PV generator topology. This relocation can be carried out by inserting a switching matrix between the PV generator and the inverter, enabling at any time the parallel connection of any PV module in any of the m rows of the PV generator, thus preserving the structure of n modules per row. This design requirement can be achieved by using $2 \cdot m \cdot n$ switches of single-pole m-throws, as shown in Fig. 2 for the case of $m = 3$ rows and $n = 3$ PV modules per row.

It can be pointed out that this structure can be expanded to increase the current and/or the voltage capabilities of the PV generator preserving the matrix structure: A current increase can be obtained by adding the same number of PV modules in each row, whereas a voltage increase will result from the addition of PV module rows to the single string.

On the other hand, the previous switching matrix enables $(m \cdot n)!$ possible reconfigurations of the PV modules (i.e., $9! = 362880$ for the case of Fig. 2). However, as shown in Fig. 3, some of the possible configurations can be disregarded since both the module position in a row [Fig. 3(a)] and the row position in the single string [Fig. 3(b)] are irrelevant with respect to the delivered dc output power.

The configurations which can deliver different values of output power, assuming that the irradiances present on each module are different, will be referred as "configurations of interest." For a PV generator with an $m \times n$ matrix structure, the number of these configurations, noted as N_{ci}, is given by

$$N_{ci} = \frac{(m \cdot n)!}{m! \cdot (n!)^m}. \tag{1}$$

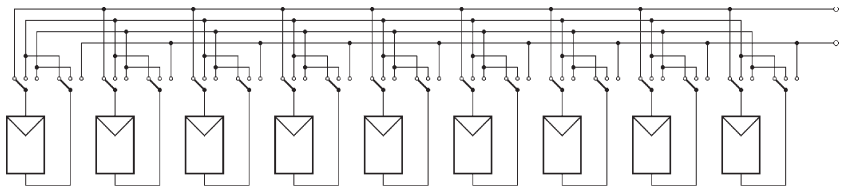

Fig. 2. Switching matrix for $m = n = 3$. General case.

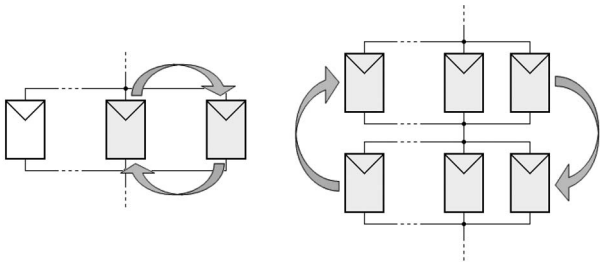

Fig. 3. Irrelevant configurations respect to the delivered dc power.

In particular, for the case where $m = n = 3$ only 280 configurations of the 362 880 ones can deliver different values of maximum dc power at the PV generator output. As a consequence, the number of switches needed to handle these 280 configurations can be reduced with respect to the general case, thus simplifying the switching matrix design. For instance, Fig. 4 shows the resulting simplified switching matrix for the previous case, where only 14 switches of 3 throws and 2 switches of 2 throws are needed instead of the 18 switches of 3 throws of Fig. 2.

III. Switching Matrix Control: Reconfiguration Strategy

The reconfiguration strategy is based on the fact that, on one hand, the maximum power point (MPP) voltage has a small variation within a wide range of the irradiance on a PV module, and, on the other hand, that the MPP current of a PV module can be considered nearly proportional to the irradiance value.

Therefore, referred to the EAR PV generator topology, it can be concluded as follows.

1) The MPP voltage of parallel-connected PV modules will not be greatly affected by the value of the irradiance on each module.
2) The current flowing through a set of parallel-connected PV modules will be almost proportional to the amount of the irradiance values present on each module.

In order to maximize the available power at the PV generator's output, it would be desirable that none of the series-connected rows of parallel-connected PV modules limits the current flowing in the single string. This behavior can be achieved if the currents, and thus the irradiances, in the different rows are similar. This principle of operation is referred as "irradiance equalization" of the PV generator. Accordingly, the reconfiguration strategy is based on relocating the PV modules on the rows so that the irradiance equalization is achieved. This principle is shown in Fig. 5, where, starting from an initial configuration [Fig. 5(a)], the strategy relocates the modules 2 and 9 to equalize the average of the irradiances present at each row [Fig. 5(b)].

The flowchart of the algorithm implementing this reconfiguration strategy is shown in Fig. 6, and its main steps are described in the following.

A. Offline Computation: Setting Initial Conditions

Starting from a PV generator formed by $m \times n$ PV modules initially connected, as shown in Fig. 1, the algorithm assumes that the irradiance value of each module is known (or can be estimated, as is addressed later) and is noted as G_{ij}, where $i = 1, \ldots, m$ and $j = 1, \ldots, n$ stand for the row and the column, respectively, where the module is initially located. Once the values of m and n are known, and assuming that all the values of the irradiance G_{ij} are different, the algorithm computes offline all the configurations of interest defined in Section II. Each of these configurations is identified as A_k, where $k = 1, 2, \ldots, K$ (note that if $m = n = 3$, then $K = 280$), and the corresponding irradiance of each module is noted as G_{ijk}.

B. Online Computation

1) Irradiance Estimation: The reconfiguration algorithm requires the knowledge of the irradiance on each module. Even though this parameter can be known by means of an irradiance sensor, it can alternatively be estimated from the measurements of the PV module voltage and current and the simplified solar panel electrical model given by

$$G_{ij} = \alpha \cdot \left[I_{ij} + I_0 \cdot (e^{V_{ij}/nV_T} - 1) \right] \tag{2}$$

being G_{ij} the estimated irradiance, I_{ij} and V_{ij} the measured current and voltage, respectively, and α, I_0, and nV_T a set of parameters which can be evaluated from the values of the short-circuit current, the open-circuit voltage, and the maximum power operating point of the PV module given in the data sheets of the manufacturer, respectively. As it is addressed in the next section, this option has been finally selected for the reconfigurable PV system design since from the measurements of the voltage and the current of each module a possible module failure can also be detected and taken into account by the reconfiguration algorithm to try to minimize the corresponding loss of dc power.

2) Computation of Average Irradiance Present at Each Row: For each of the configurations of interest A_k, the algorithm computes the average irradiance on the n parallel-connected

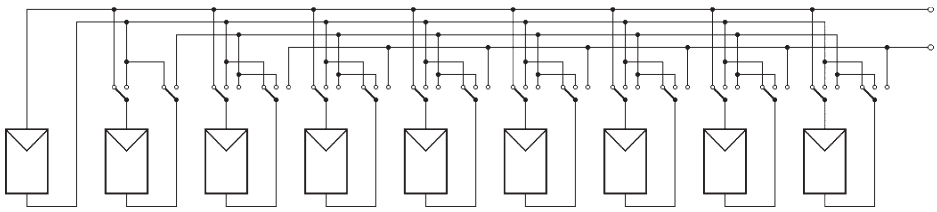

Fig. 4. Simplified switching matrix for $m = n = 3$.

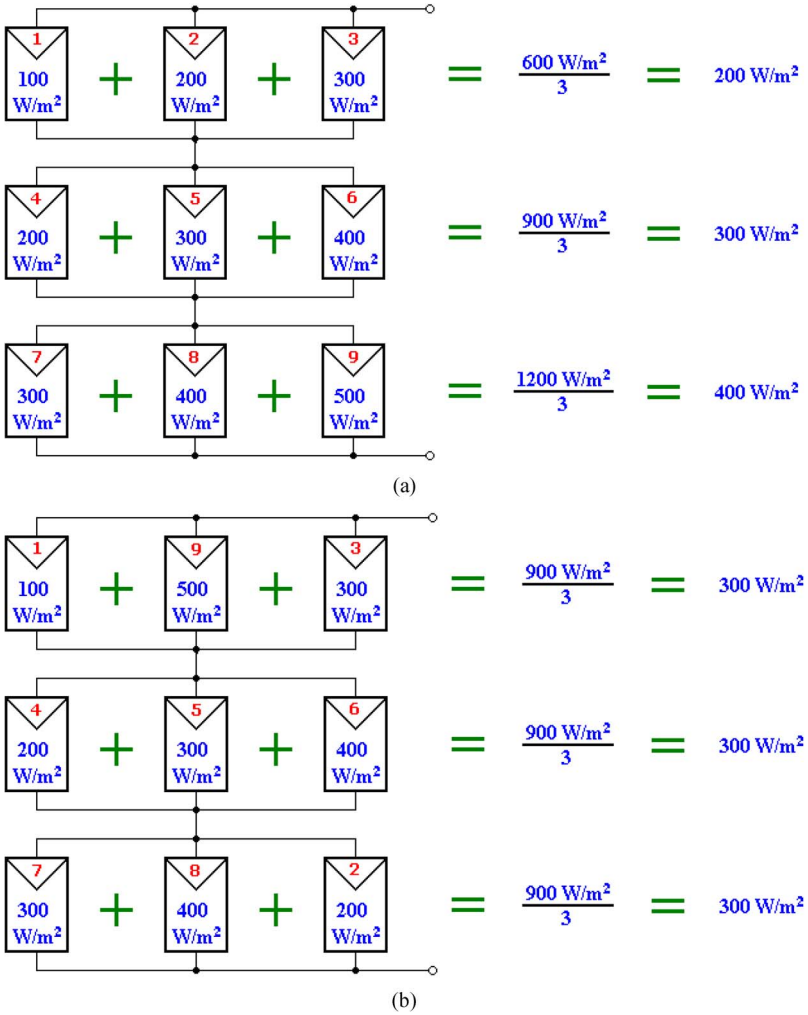

Fig. 5. Principle of the reconfiguration strategy. (a) Initial configuration. (b) Final configuration.

modules of each row. If G_{ik} stands for the average irradiance present at the row i of the configuration A_k, the algorithm computes

$$G_{ik} = \frac{\sum_{j=1}^{n} G_{ijk}}{n}, \qquad i = 1, 2, \ldots, m \quad k = 1, 2, \ldots, K. \tag{3}$$

3) Computation of "Irradiance Equalization Index": In order to subsequently check which of the configurations of interest will deliver the maximum power, the algorithm computes for each configuration a merit factor called "irradiance equalization index." This index is defined to quantify how different are the average irradiances present at each row and consequently what is the degree of current limitation of the configuration. Even other definitions are possible, a simple way to define the irradiance equalization index of the configuration A_k, referred as $M_{\mathrm{IE}}(A_k)$ is

$$M_{\mathrm{IE}}(A_k) = \max[G_{1k}, G_{2k}, \ldots, G_{mk}] - \min[G_{1k}, G_{2k}, \ldots, G_{mk}] \tag{4}$$

consequently, the algorithm computes

$$M_{\mathrm{IE}}(A_k) = \max[G_{1k}, G_{2k}, \ldots, G_{mk}] - \min[G_{1k}, G_{2k}, \ldots, G_{mk}] \quad \text{for} \quad k = 1, \ldots, K. \tag{5}$$

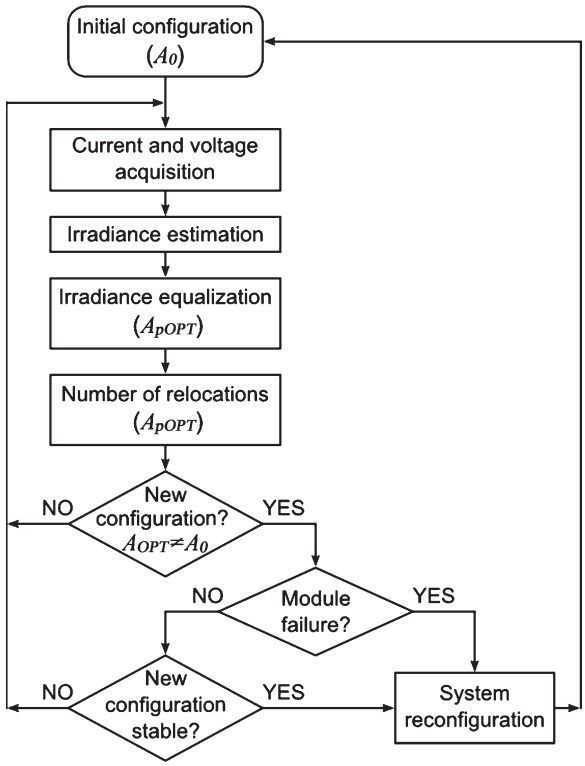

Fig. 6. Flowchart of the algorithm for the system reconfiguration.

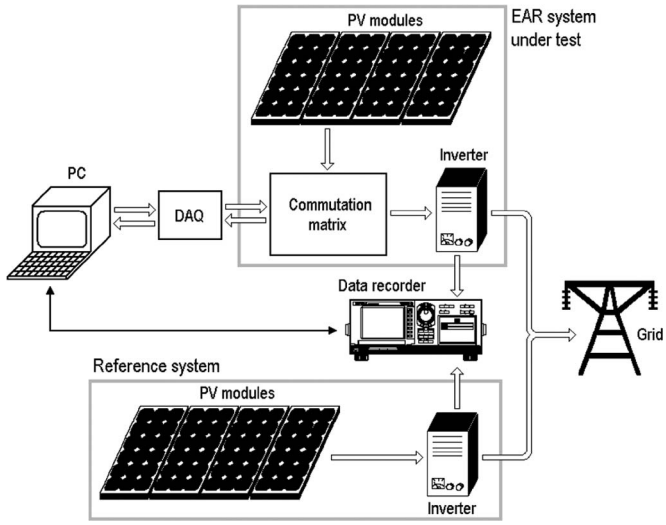

Fig. 7. Experimental setup.

It can be noted that the better the irradiance equalization, the lower the index value. In particular, if all the rows of a configuration exhibit the same average irradiance (i.e., irradiance equalized for each row), then, $M_{\mathrm{IE}}(Ak) = 0$, as in the case of a PV generator operating under an uniform irradiance.

As previously mentioned, the computation of $M_{\mathrm{IE}}(A_k)$ allows the algorithm to detect what configurations are optimal as regards the delivered maximum power. These configurations, noted as A_{pOPT} being p an integer, constitute a subset of the configurations of interest, namely, $A_{\mathrm{pOPT}} \in \{A_1, A_2 \ldots, A_K\}$ and can easily be detected by computing

$$M_{\mathrm{IE}}(A_{\mathrm{pOPT}}) = \min\left[M_{\mathrm{IE}}(A_1), M_{\mathrm{IE}}(A_2), \ldots, M_{\mathrm{IE}}(A_K)\right]. \tag{6}$$

It can be pointed out that more than one configuration can result optimal.

4) Computation of Number of PV Module Relocations: In order to minimize the number of relocations, the algorithm computes for each optimal configuration a second merit factor defined as "number of relocations."

This index evaluates the number of modules to be relocated when the PV generator is reconfigured from the current configuration A_0 to the optimal one under analysis, A_{pOPT}. For instance, referring to Fig. 5, the "number of relocations" to carry out the reconfiguration from the initial configuration of Fig. 5(a) to the optimal one in Fig. 5(b) is two, and corresponds to the relocations of modules 2 and 9.

These previous steps will allow us to identify the optimal configuration noted as A_{OPT}, i.e., the configuration that concurrently better equalizes the irradiance and minimizes the number of module relocations. In the next step, the algorithm decides if the reconfiguration has to take place or not, as described in the following.

5) Reconfiguration Decision Making: As can be seen in the algorithm flowchart, the decision making is structured in three hierarchical levels, namely, as follows.

The first level of decision disables the reconfiguration of the switching matrix if the optimum configuration is the same that the initial one. Otherwise, the algorithm goes to the second decision level.

The second level asks for a possible module failure which can be detected from the measurement of the module current: If any module is in open circuit, the reconfiguration takes place immediately to avoid the possible disconnection of the PV generator at the inverter's input. Otherwise, the algorithm goes to the third decision level.

The third decision level enables the reconfiguration of the switching matrix only if the optimum configuration is stable (i.e., if it remains the same) during a certain amount of time. Once the optimum configuration is determined for the first time, the algorithm runs a prefixed number of turns and checks if this configuration remains unchanged to authorize the reconfiguration. Referring to the system implementation described later, the algorithm running time spends around 200 ms in one turn, including the data acquisition, the irradiance estimation, and the irradiance equalization procedure leading to the optimum configuration. In the third decision level, the algorithm has been programmed to run during 15 s, which means that the optimum configuration is recalculated 75 times before the reconfiguration takes place. As will be evidenced later by experimental results, this strategy avoids a large number of reconfigurations in front of fast irradiance changes on the PV generator, as in the case of cloudy days, and thereby preserves the lifetime of the switches.

In order to experimentally validate the assumptions above under a proof of concept basis, the next section describes a work bench formed by a 1.65-kWp PV grid-connected system including a switching matrix controlled by the irradiance equalization algorithm summarized previously.

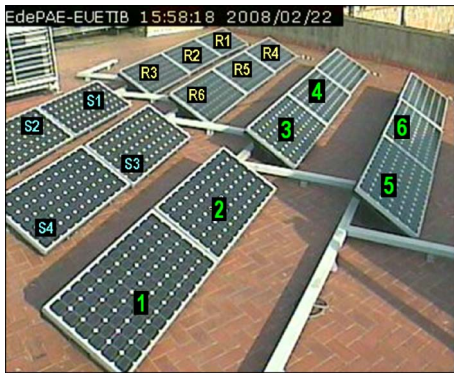

Fig. 8. Modules layout of the PV system. [R1. . .R6] Reference system. [S1. . .S4] Static section. [1. . .6] Reconfigurable section.

IV. Experimental Setup

A. General Description

The setup shown in Fig. 7 has been built using commercial equipment, and includes a PV grid-connected reference system used to check the irradiance evolution during the tests, the EAR reconfigurable one, and processing and monitoring devices.

The setup components are described in the following.

1) Reference PV grid-connected system.
   a) Five PV modules STP165S-24/Aa (825 W_P).
   b) SB700 inverter from SMA (700 W).
2) Processing and monitoring facilities.
   a) Personal computer which embeds the control algorithm and manages the recorded data.
   b) Data acquisition system USB-6259 DAQ from *National Instruments*.
   c) WT1600 power meter from *Yokogawa.*
3) EAR PV system under test.
   a) Relay-based switching matrix.
   b) Ten PV modules STP165S-24/Aa (1650 W_P). Each module includes 72 series-connected solar cells and two parallel-connected bypass diodes (one for each set of 36 cells).
   c) SB1100 inverter from SMA (1100 W), including an MPPT algorithm that only runs within the inverter input voltage operating range, namely, from 139 to 400 V.

B. EAR PV Generator Design

In order to comply with the SB1100 inverter input voltage and current operating ranges, and to build a switching matrix of reduced size, the EAR PV generator includes a static section of four PV modules and a reconfigurable one of six modules formed by three series-connected rows of two parallel-connected modules per row, leading to a 3×2 matrix structure. Fig. 8 shows the layout of the reconfigurable system with its static and reconfigurable parts as well as the reference system.

On the other hand, Fig. 9 shows the EAR PV generator configuration and the location of the auxiliary circuits to sense the current and the voltage of each module. In this regard, the voltage measurements are referred to a common node, to avoid the use of differential amplifiers requiring high common mode rejection ratio values.

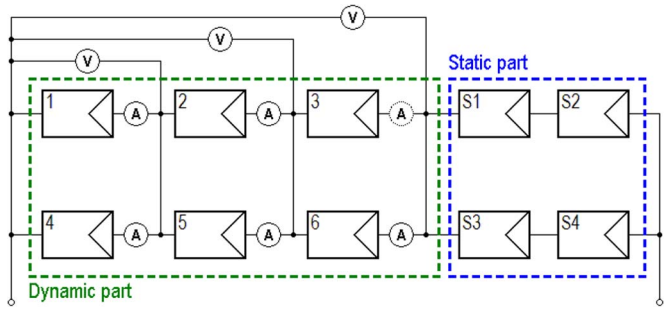

Fig. 9. EAR PV generator under test with the static section, the reconfigurable one, and the voltage and current sensors distribution.

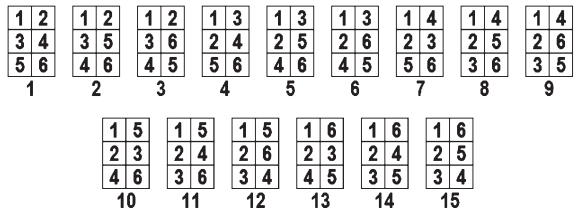

Fig. 10. Fifteen PV modules configurations of interest.

It can be noted that one current sensor can be omitted, since one current value comes from the application of Kirchoff laws.

C. Switching Matrix and Auxiliary Circuits Design

As addressed in the previous section, the switching matrix simplified design first requires the analysis of which configurations are of interest, i.e., which of them deliver different values of output dc power. For the case of study, $m = 3$ and $n = 2$, thus only 15 configurations are of interest (i.e., A_k with $k = 1, 2, \ldots, 15$) among the $(3 \cdot 2)! = 720$ possible ones. Fig. 10 shows the location of the modules (numbered from one to six) in the reconfigurable part of the EAR PV generator for each of these 15 configurations, where the PV modules in the same row are parallel connected and the three rows of PV modules are series connected.

The simplified switching matrix enabling the parallel-connection of any PV module in any row is shown in Fig. 11 and includes two single-pole double-throw and four single-pole triple-throw switches.

Switching relays are good candidates to the implementation of these switches due to their control simplicity and the inherent electrical isolation operation of their control circuitry. From an efficiency point of view, bistable relays (or latching relays) are particularly well suited since they only spend energy to change their state. However, electromagnetic monostable relays have been finally included in the prototype since they control results simpler.

The electrical architecture of the system is based on single dc bus connecting, on one hand, the static section and the inverter [see Fig. 12(a)]. On the other hand, the bus also feeds the switching matrix relays and the auxiliary circuits. Fig. 12(b) shows the dc bus, the six switches driving a single module connection as well as its corresponding current sensing circuitry

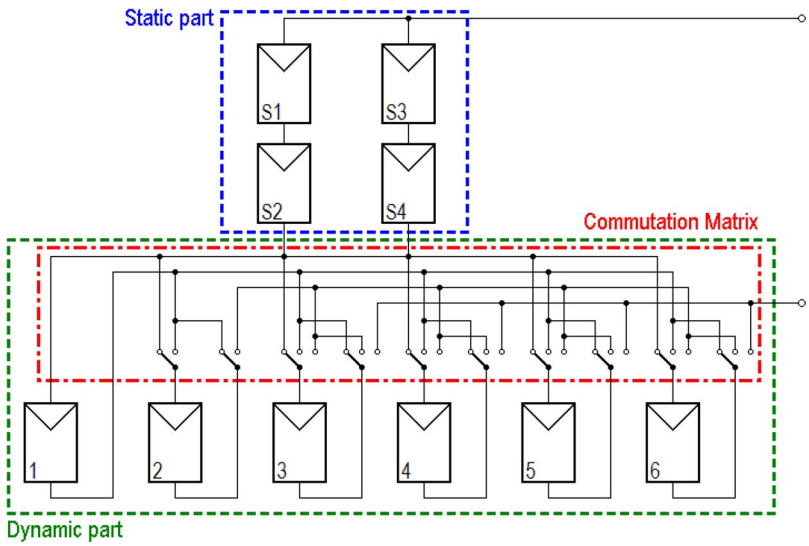

Fig. 11. EAR PV generator under test with the static section, the dynamically reconfigurable one, and the simplified commutation matrix.

implemented by means of a Hall-effect current transducer. Fig. 12(c) shows the voltage measurement circuitry across the module terminals (see also Fig. 8).

The PV modules current and voltage measured values are sent through the USB-6259 DAQ to the PC which subsequently computes using MATLAB software the reconfiguration algorithm driving the switching matrix.

As previously reported in Section III, the algorithm running time spends around 200 ms in one turn.

Finally, the dc output power of the reference system and the EAR one is measured and registered for offline analysis by means of the WT1600 power meter. In this regard, since both grid-connected inverters include their own MPPT algorithm, it is assumed that the measured static output dc power corresponds to the maximum one.

V. Experimental Results

Three tests have been performed to check the proper operation of the equalization irradiance algorithm and the subsequent reconfiguration of the solar array.

1) The first one artificially shades several PV generator modules.
2) The second one emulates the failure of several PV modules by disconnecting them from the PV generator.
3) The third one registers the daily operation of both systems, in order to evaluate the shadowing effect on the PV generator due to the surrounding buildings.

The identification of the EAR PV modules and the configurations of interest addressed in these tests correspond to the numeration given in Fig. 9. The initial connection of the modules corresponds to the configuration 1 of Fig. 10. The obtained results are described next:

A. PV Generator Operating Under Partial Shades

This test artificially shades one, two, or three modules of the EAR PV generator and drives the matrix to sequentially implement the 15 configurations of interest.

The power to voltage curve of each PV generator configuration is obtained to evidence the existence of optimal configurations that exhibit a maximum within the MPPT voltage window where the inverter operates (the lower limit of this window is shown in the curves and is noted as $V_{\mathrm{MPP\text{-}min}}$).

Fig. 13(a) corresponds to the case where a single module is shaded (module 1 in Fig. 9); as it can be seen, none of the 15 configurations results optimal since all the configurations lead to the same $P-V$ curve. In contrast, Fig. 13(b) and (c) corresponds to the tests when the modules 1 and 4, and the modules 1, 4, and 6 are, respectively, shaded, and show that, in both cases, several configurations exhibit a maximum within the MPPT voltage window, and thereby result optimal. Referring to Fig. 10, these optimal configurations correspond to the case when the shaded modules are not parallel connected in the same row.

B. Modules Failure in PV Generator

For this test, the modules disconnection sequence shown in Table I is applied. This sequence emulates the failure of several modules of the PV generator.

Fig. 14 shows the measured dc output power of both the reference PV system and the EAR PV system under test when the switching matrix control is as follows: 1) activated and 2) disabled. These measurements evidence the power improvement of the EAR PV generator.

C. PV Generator Daily Operation

Two tests have been carried out to evaluate the EAR system daily operation: The first one, previously reported in [20], focuses on the energy balance improvement of the system and the second one checks the number of reconfigurations under different weather conditions to evaluate the operation of the reconfiguration algorithm as regards the switches lifetime. These tests are described next.

1) Energy Improvement: This test is devoted to quantify the daily energy improvement of the EAR-based system, when

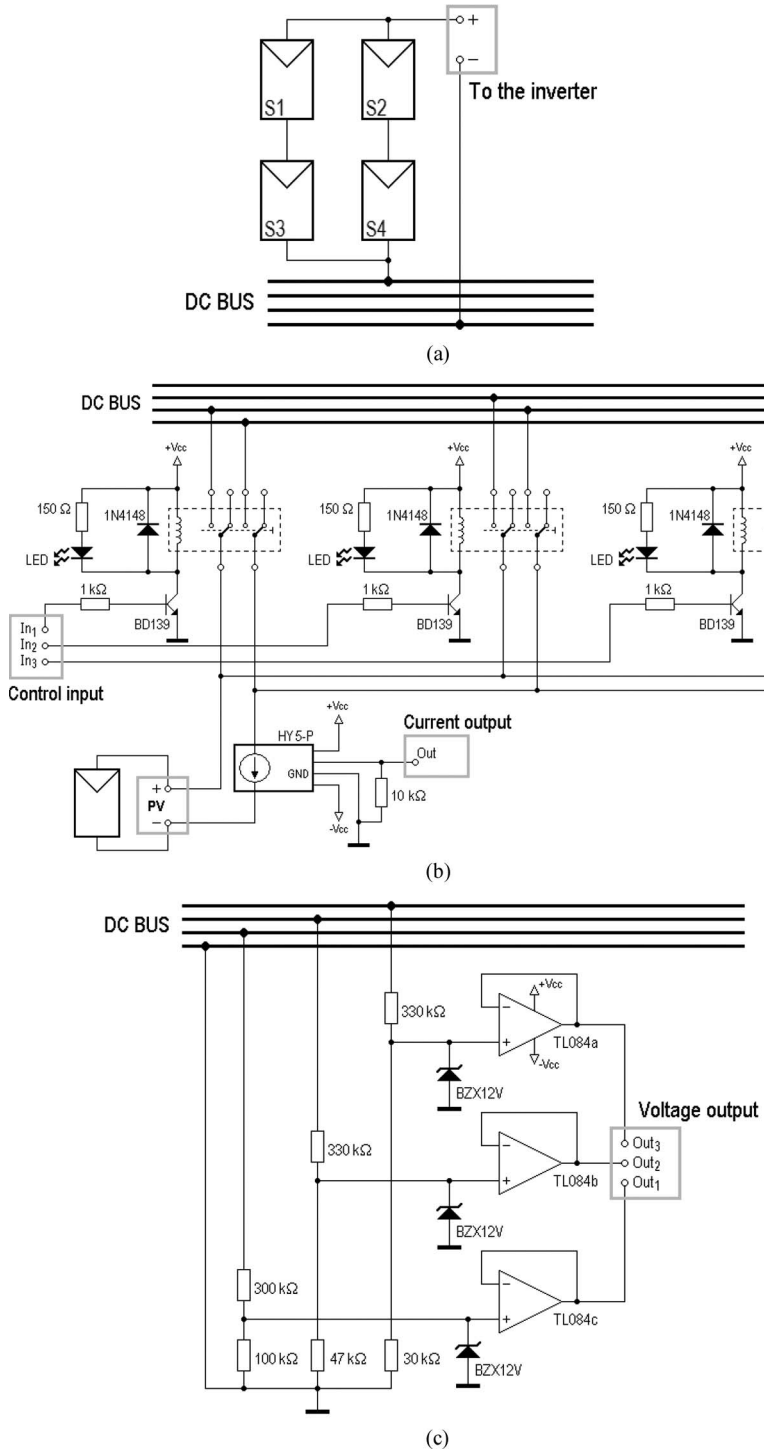

Fig. 12. Electrical architecture of the EAR PV generator.

the PV generator is affected by the shadows coming from the surrounding buildings. Nevertheless, the available PV panels at the laboratory are not enough to build both a static PV system and an EAR-based reconfigurable one which are required for a simultaneous comparison. Alternatively, this comparison has been done over the single EAR-based system during two consecutive sunny days of similar irradiance levels, enabling the switching matrix control during the first day, and disabling it during the second one in order to emulate a nonreconfigurable (i.e., static) PO PV system.

Fig. 15(a) shows the output power evolution during the day 02-22-2008 where the switching matrix control is enabled and reconfigures the PV generator according to the equalization irradiance algorithm. Similarly, Fig. 15(b) shows the output power of the day 02-23-2008 where the switching matrix control disabled.

It is worth noting that the energy consumption of the EAR system must be subtracted from the measured value of $E_{\mathrm{EAR_{ON}}}$ since in the present design this system is not supplied by the PV modules. However, a measurement of the laboratory

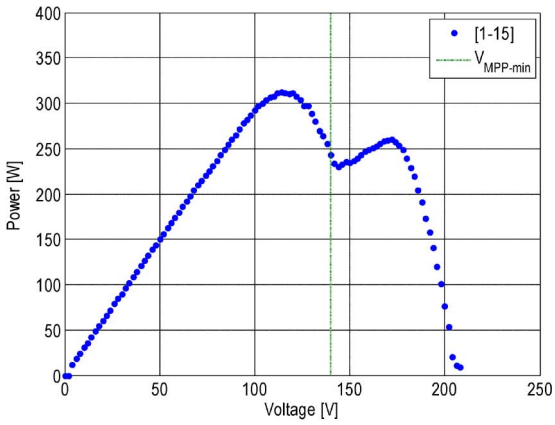

(a)

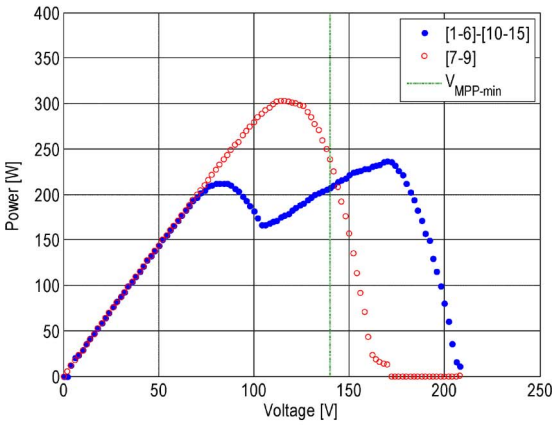

(b)

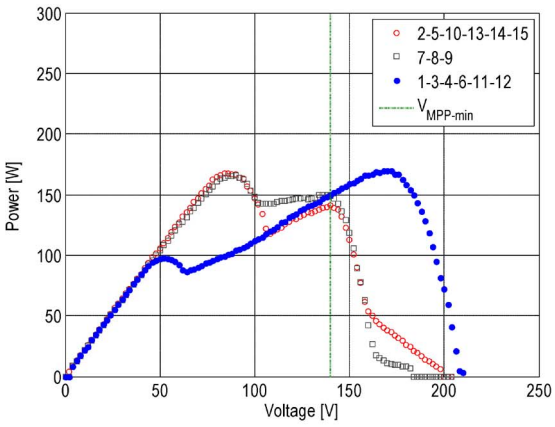

(c)

Fig. 13. Output power for EAR PV system under conditions of shadow. (a) Shadow on module number 1. (b) Shadow on modules number 1 and 4. (c) Shadow on modules number 1, 4, and 6.

TABLE I
SEQUENCE FOR PV MODULES FAILURE EMULATION

Time (s)	Action
0	System connection with configuration n° 1
20	Module 1 disconnection
40	Module 2 disconnection
60	Module 6 disconnection
80	Module 6 reconnection
100	Module 2 reconnection
120	Module 1 reconnection
140	End of test

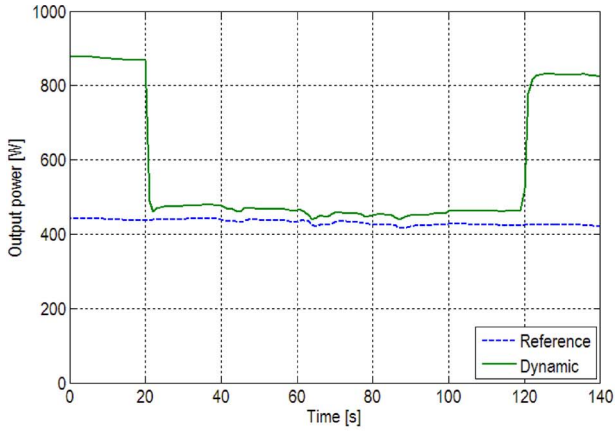

(a)

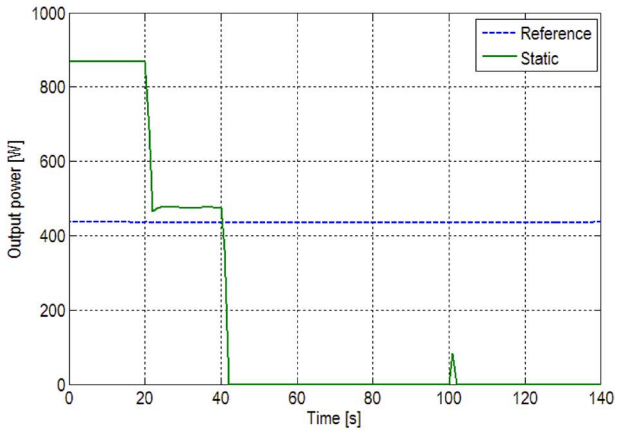

(b)

Fig. 14. EAR PV system output power when the switching matrix control is as follows: (a) activated and (b) disabled.

prototype consumption may not be representative since the reconfiguration algorithm has been implemented on a PC, and monostable relays have been used instead of bistable ones. Alternatively, assuming the same implementation as presented previously but based on bistable relays and where the PC is replaced by a low-cost microcontroller, the EAR system power consumption can be estimated from the data sheets of manufacturers. In this regard, two kinds of power consumptions can be estimated, namely, as follows.

1) Standby power consumption: This refers to the consumption of the data acquisition system, the sensors/conditioning circuits, and that corresponding to a low-cost microcontroller, for instance, the ATmega16 from ATMEL. The overall consumption of this equipment can be estimated around 1.2 W. Accordingly, if the PV system operates during 16 h a day in average, the standby energy consumption value can be estimated around 20 W · h a day. This consumption is the minimum one required by the EAR system to operate even if no reconfiguration takes place.
2) Bistable relay switching consumption: A change of the relay state requires about 20 W during 20 ms [21], [22], which means a power consumption of 0.12 mW · h per switching. This value can be neglected since at least 2000 switches a day would be required to spend less than 1% of the standby power consumption.

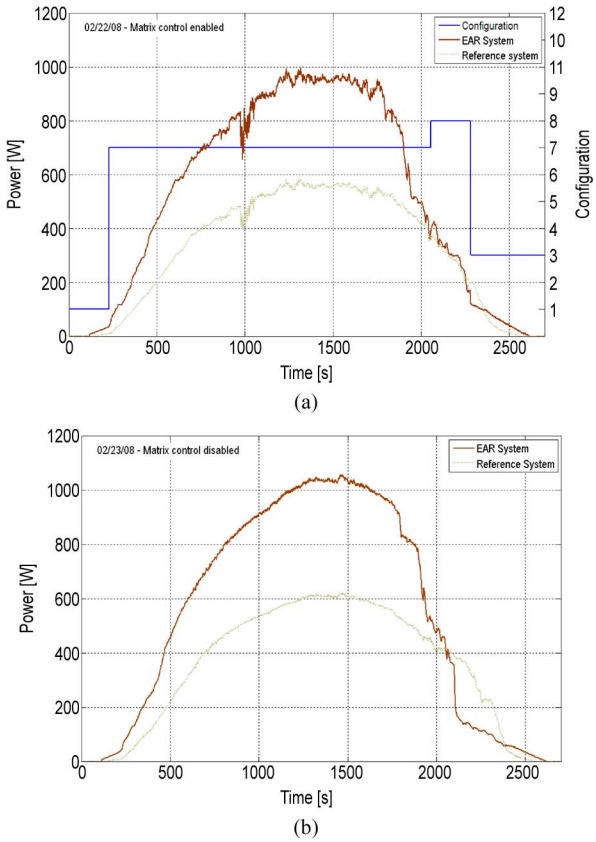

Fig. 15. Output power of EAR system and reference system when the control of the EAR system is as follows: (a) enabled and (b) disabled.

TABLE II
ENERGY DELIVERED TO MAINS FOR PV SYSTEMS

System	Energy delivered to the mains	
	Day 1 (02-22-08) Control enabled	Day 2 (02-23-08) Control disabled
EAR	$E_{EAR_{ON}} = 5752.7\,Wh$	$E_{EAR_{OFF}} = 6025.4\,Wh$
Reference	$E_{REF_1} = 3539.0\,Wh$	$E_{REF_1} = 3818.7\,Wh$

The energy injected to the mains during each of these two days taking into account these power consumption estimations, is reported in Table II, where $E_{\mathrm{EAR_{ON}}}$ and $E_{\mathrm{EAR_{OFF}}}$ stand for the delivered energy when the switching matrix control is enabled or disabled, respectively.

From the results of Table II, it must be pointed out that the absolute values of the delivered energy by the EAR system when the switching matrix is either enabled or disabled cannot be directly compared since the irradiance level evolution is not strictly the same during the two days, as it can be checked from the energy values of the reference system. In this regard, the comparison can be made by using the normalized energy values of the EAR system with respect to the corresponding reference ones, namely

$$\frac{E_{\mathrm{EAR_{ON}}}}{E_{\mathrm{REF_1}}} = 1.626 \quad \frac{E_{\mathrm{EAR_{OFF}}}}{E_{\mathrm{REF_2}}} = 1.578 \tag{7}$$

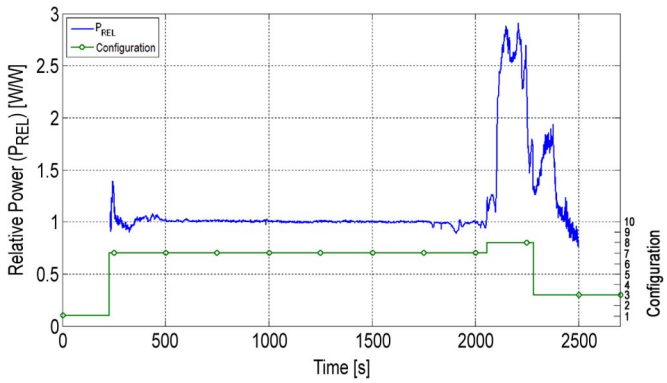

Fig. 16. EAR PV system relative output power.

which means that the EAR-based reconfigurable system delivers $1-(1.578/1.626)\approx 3\%$ more energy than the static one.

Alternatively, the comparison can also be performed in terms of the output power evolution, by comparing the output power of the static PV generator with that of the reconfigurable one, scaled by the power ratio of the reference system during the two days, namely: If $P_{\mathrm{EAR_{ON}}}(t)$ and $P_{\mathrm{EAR_{OFF}}}(t)$ stand for the EAR system power evolution when the switching matrix control is enabled or disabled, respectively, and and $P_{\mathrm{REF_1}}(t)$, $P_{\mathrm{REF_2}}(t)$ correspond to the power evolution of the reference system during the two days, the relative power $P_{\mathrm{REL}}(t)$ can be defined as

$$\left.\begin{aligned} P_{\mathrm{REL_{ON}}}(t) &= \frac{P_{\mathrm{EAR_{ON}}}(t)}{P_{\mathrm{REF1}}(t)} \\ P_{\mathrm{REL_{OFF}}}(t) &= \frac{P_{\mathrm{EAR_{OFF}}}(t)}{P_{\mathrm{REF2}}(t)} \end{aligned}\right\} \Rightarrow P_{\mathrm{REL}}(t) = \frac{P_{\mathrm{REL_{ON}}}(t)}{P_{\mathrm{REL_{OFF}}}(t)}. \tag{8}$$

Fig. 16 shows the output power evolution of $P_{\mathrm{REL}}(t)$, where the results at the beginning and end of the day are not representative due to overflow phenomena in the computation procedure.

It is worth noting that the plots of power evolution give us more information about the reconfiguration process: As it can be seen from Figs. 15 and 16, the power increase of the EAR system starts around $t = 2050$ s, when the EAR PV generator is reconfigured from combination 7 to 8, and around $t = 2300$ s, when the system is reconfigured from combination 8 to 3. The proper operation of the reconfiguration algorithm is confirmed by Fig. 8 which shows the shades distribution over the EAR generator coming from the surrounding buildings at $t = 2050$ s when the first relevant reconfiguration takes place.

As it can be seen, panels 5 and 6 are fully and partially shaded, respectively; since, referring to Fig. 9, the initial combination of the EAR PV generator is the number 7, both panels are parallel connected, thus limiting the overall current of the PV generator. The reconfiguration algorithm then chooses the combination number 8 where both panels are now series connected, in order to improve the PV generator output power by relaxing the previous current limitation.

2) Number of Reconfigurations Under Different Weather Conditions: The EAR system has been monitoring during one week where the weather was variable, including both sunny and

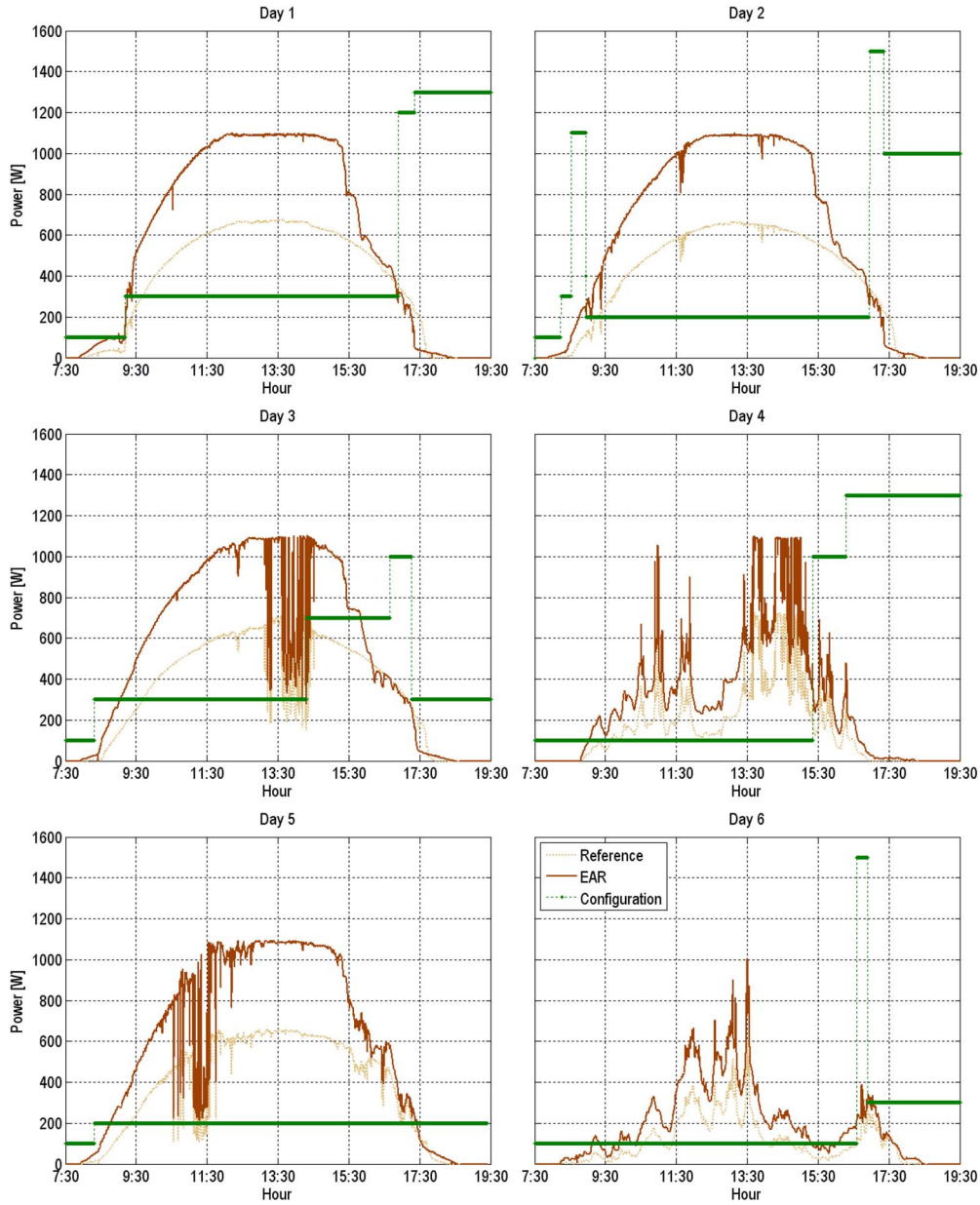

Fig. 17. Output power of EAR and reference system.

cloudy days. Fig. 17 shows the power evolution of both the reference system and the EAR one. As it can be seen, at most five reconfigurations have been taken place during the day 02. It can be concluded that the number of reconfigurations in this test remains low.

VI. Conclusion

This paper has suggested a PV generator reconfiguration strategy to improve the power of commercial PO grid-connected PV systems available nowadays, formed by standard PV modules and a single central inverter driven by a conventional MPPT algorithm. This strategy is implemented by means of a controllable matrix of switches configuring the PV modules in a single-string of parallel-connected rows connected to the central inverter. A set of experimental results carried out under a proof of concept basis on a small-scale grid-connected PV system of 1.65 kWp has shown both the feasibility of the approach and the resulting improvement of the delivered power under partial shades or in case of module failures.

In spite of the disadvantages derived from its greater complexity and cost, the power loss mitigation of this approach can result interesting for small-scale installations in urban environments where the PV generator can work under conditions of severe partial shadows projected by surrounding obstacles.

Finally, it can be pointed out that given a switching matrix size (i.e., defined by the number of switches), the installed PV power can be expanded since the same matrix can also handle associations of hard-wired series-parallel modules instead of single ones, this being a subject of further research.

The main results of this paper are pending a Spanish patent under Reference P200802082.

REFERENCES

[1] M. Meinhardt and G. Cramer, "Past, present and future of grid connected photovoltaic and hybrid power systems," in *Proc. IEEE Power Eng. Soc. Summer Meeting*, Seattle, WA, Jul. 2000, vol. 2, pp. 1283–1288.

[2] S. B. Kjaer, J. K. Pedersen, and F. Blaabjerg, "A review of single-phase grid-connected inverters for photovoltaic modules," *IEEE Trans. Ind. Appl.*, vol. 41, no. 5, pp. 1292–1306, Sep./Oct. 2005.

[3] G. Petrone, G. Spagnuolo, R. Teodorescu, M. Veerachary, and M. Vitelli, "Reliability issues in photovoltaic power processing systems," *IEEE Trans. Ind. Electron.*, vol. 55, no. 7, pp. 2569–2580, Jul. 2008.

[4] H. Pang, J. Close, and K.-H. Lam, "Evaluation of relative importance of factors affecting the performance of a local grid-connecting BIPV system by computer simulation," in *Proc. 3rd World Conf. Photovoltaic Energy Convers.*, Osaka, Japan, May 2003, vol. 3, pp. 2439–2442.

[5] N. J. C. M. van der Borg and M. J. Jansen, "Energy loss due to shading in a BIPV application," in *Proc. 3rd World Conf. Photovoltaic Energy Convers.*, Osaka, Japan, May 2003, vol. 3, pp. 2220–2222.

[6] M. Drif, P. J. Pérez, J. Aguilera, and J. D. Aguilar, "A new estimation method of irradiance on a partially shaded PV generator in grid-connected photovoltaic systems," *Renew. Energy*, vol. 33, no. 9, pp. 2048–2056, Sep. 2008.

[7] C. Rodriguez and G. A. J. Amaratunga, "Long-lifetime power inverter for photovoltaic AC modules," *IEEE Trans. Ind. Electron.*, vol. 55, no. 7, pp. 2593–2601, Jul. 2008.

[8] B. Sahan, A. N. Vergara, N. Henze, A. Engler, and P. Zacharias, "A single-stage PV module integrated converter based on a low-power current-source inverter," *IEEE Trans. Ind. Electron.*, vol. 55, no. 7, pp. 2602–2609, Jul. 2008.

[9] E. Roman, R. Alonso, P. Ibanez, S. Elorduizapatarietxe, and D. Goitia, "Intelligent PV module for grid-connected PV systems," *IEEE Trans. Ind. Electron.*, vol. 53, no. 4, pp. 1066–1073, Aug. 2006.

[10] N. Femia, G. Lisi, G. Petrone, G. Spagnuolo, and M. Vitelli, "Distributed maximum power point tracking of photovoltaic arrays: Novel approach and system analysis," *IEEE Trans. Ind. Electron.*, vol. 55, no. 7, pp. 2610–2621, Jul. 2008.

[11] J. A. Barrena, L. Marroyo, M. A. R. Vidal, and J. R. T. Apraiz, "Individual voltage balancing strategy for PWM cascaded H-bridge converter-based STATCOM," *IEEE Trans. Ind. Electron.*, vol. 55, no. 1, pp. 21–29, Jan. 2008.

[12] M. Calais, J. Myrzik, T. Spooner, and V. G. Agelidis, "Inverters for single-phase grid connected PV systems—An overview," in *Proc. IEEE 33rd Annu. PESC*, Cairns, Australia, Jun. 2002, vol. 4, pp. 1995–2000.

[13] D. Nguyen and B. Lehman, "An adaptive solar photovoltaic array using model-based reconfiguration algorithm," *IEEE Trans. Ind. Electron.*, vol. 55, no. 7, pp. 2644–2654, Jul. 2008.

[14] Y. Auttawaitkul, B. Pungsiri, K. Chammongthai, and M. Okuda, "A method of appropriate electric array reconfiguration management for photovoltaic powered car," in *Proc. IEEE APCCAS*, Chiangmai, Thailand, Nov. 1998, pp. 201–204.

[15] Z. M. Salameh and C. Liang, "Optimum switching point for array reconfiguration controllers," in *Proc. IEEE 21st PVSEC*, Kissimmee, FL, May 1990, vol. 2, pp. 971–976.

[16] Z. M. Salameh and F. Dagher, "The effect of electrical array reconfiguration on the performance of a PV-powered volumetric water pump," *IEEE Trans. Energy Convers.*, vol. 5, no. 4, pp. 653–658, Dec. 1990.

[17] Z. Salameh, A. K. Mulpur, and F. Dagher, "Two-stage electrical array reconfiguration controller for PV-powered water pump," *Sol. Energy*, vol. 44, no. 1, pp. 51–56, 1990.

[18] G. Velasco, J. J. Negroni, F. Guinjoan, and R. Piqué, "Energy generation in PV grid-connected systems: A comparative study depending on the PV generator configuration," in *Proc. IEEE ISIE*, Dubrovnik, Croatia, Jun. 2005, vol. 3, pp. 1025–1030.

[19] G. Velasco, J. J. Negroni, F. Guinjoan, and R. Piqué, "Irradiance equalization method for output power optimization in plant oriented grid-connected PV generators," in *Proc. 11th Eur. Conf. Power Electron. Appl., EPE*, Dresden, Germany, Sep. 2005.

[20] G. Velasco, F. Guinjoan, and R. Piqué, "Grid-connected PV systems energy extraction improvement by means of an Electric Array Reconfiguration (EAR) strategy: Operating principle and experimental results," in *Proc. IEEE PESC*, Rhodes, Greece, Jun. 2008, pp. 1983–1988.

[21] Gruner AG, Product Range: Latching Relays. [Online]. Available: www.gruner.de

[22] Arteche Group, Latching Relays Documentation. [Online]. Available: www.arteche.com

Guillermo Velasco-Quesada (S'04–M'09) was born in Barcelona, Spain. He received the Ingeniero Técnico Industrial en Electricidad, the Ingeniero en Electrónica, and the Doctor en Ingeniería Electrónica degrees from the Universitat Politècnica de Catalunya (UPC), Barcelona, in 1990, 2002, and 2008, respectively.

Since 1992, he has been an Associate Professor with the Departamento de Ingeniería Electrónica, Escuela Universitaria de Ingeniería Técnica Industrial de Barcelona, UPC, where he teaches analog and power electronics. His main research interest includes analysis, modeling and control of power systems for renewable energy applications, and grid-connected PV systems based on reconfigurable topologies.

Dr. Velasco-Quesada is a member of the IEEE Industrial Electronics and IEEE Power Electronics Societies, and researcher with the Energy Processing and Integrated Circuits Group and the Power Electronics Research Center of the UPC.

Francisco Guinjoan-Gispert (M'92) received the Ingeniero de Telecomunicación and the Doctor Ingeniero de Telecomunicación degrees from the Universitat Politècnica de Catalunya (UPC), Barcelona, Spain, in 1984 and 1990, respectively, and the Docteur es Sciences degree from the Université Paul Sabatier, Toulouse, France, in 1992.

He is currently an Associate Professor with the Departamento de Ingenieria Electrónica, Escuela Técnica Superior de Ingenieros de Telecomunicación de Barcelona, UPC, where he teaches power electronics. His research interest includes power electronics modeling and control for renewable energy systems.

Dr. Guinjoan-Gispert is a member of the IEEE Industrial Electronics and IEEE Power Electronics Societies, and researcher with the Energy Processing and Integrated Circuits Group and the Power Electronics Research Center of the UPC.

Robert Piqué-López (S'82–M'86) was born in Mataró, Spain. He received the Ingeniero Técnico Industrial en Electricidad, the Ingeniero Industrial en Electricidad orientación Electrónica, and the Doctor Ingeniero Industrial degrees from the Universitat Politècnica de Catalunya (UPC), Barcelona, Spain, in 1978, 1985, and 1993, respectively.

He is currently an Associate Professor with the Departamento de Ingeniería Electrónica, Escuela Universitaria de Ingeniería Técnica Industrial de Barcelona, UPC, where teaches courses on power electronics: simulation and control. His research interests include static conversion techniques, modeling, and control for power electronics and renewable energy systems.

Dr. Piqué-López is member of the IEEE Power Electronics and Education Societies, and researcher with the Energy Processing and Integrated Circuits Group and the Power Electronics Research Center of the UPC.

Manuel Román-Lumbreras (M'09) was born in Gallur, Spain, in 1945. He received the Ingeniero Industrial en Electricidad and the Doctor Ingeniero Industrial degrees from the Universitat Politècnica de Catalunya (UPC), Barcelona, Spain, in 1975 and 2006, respectively.

From 1977 to 2000, he was an Assistant Professor with the UPC, and since 2001, he has been an Associate Professor with the Departamento de Ingeniería Electrónica, UPC. From 1965 to 2000, he was working in the industry, in the area of electrical energy production, railway power traction systems, ac and dc motor drives, electric power quality, and power converters for uninterruptible power supplies and active power filters. His actual research interests are power electronics, electric power network quality, converters for renewable energy systems, and digital control of power converters.

Dr. Román-Lumbreras is a member of the IEEE Industrial Electronics, IEEE Industrial Applications, and IEEE Power Electronics Societies.

Alfonso Conesa-Roca was born in Barcelona, Spain. He received the Ingeniero en Electrónica and Doctor en Ingeniería Electrónica degrees from the Universidad Politècnica de Catalunya (UPC), Barcelona, in 1998 and 2006, respectively.

He is currently an Associate Professor with the Departamento de Ingeniería Electrónica, Escuela Universitaria de Ingeniería Técnica Industrial de Barcelona, UPC. His current research interests include switching-mode power supplies, power architectures, resonant conversion, and photovoltaic applications.